Article

Ability of Deep Eutectic Solvent Modified Oat Straw for Cu(II), Zn(II), and Se(IV) Ions Removal

Jelena Dimitrijević [1,*] **, Sanja Jevtić** [2] **, Aleksandar Marinković** [2] **, Marija Simić** [1] **, Marija Koprivica** [1] **and Jelena Petrović** [1]

1 Institute for Technology of Nuclear and Other Mineral Raw Materials, 86 Franchet d'Esperey St., 11000 Belgrade, Serbia
2 Faculty of Technology and Metallurgy, University of Belgrade, Karnegijeva 4, 11000 Belgrade, Serbia
* Correspondence: j.dimitrijevic@itnms.ac.rs; Tel./Fax: +381-11-3691-722

Abstract: In the proposed study, agro-waste biomass oat straw (OS) was considered a potential adsorbent for Cu(II), Zn(II), and Se(IV) removal from aqueous solutions. In order to obtain material with better adsorption abilities, the OS was modified by a deep eutectic solvent (DES). Structural changes caused by the applied modification route were considered by pHpzc, SEM, FTIR, and DSC/TG analysis. These methods discovered that lignocellulosic biomass degradation and material functionalization were achieved by DES treatment. Preliminary adsorption tests showed an over fourfold increase in capacity upon modification. The kinetic parameters implied that adsorption on modified material followed the pseudo-second-order kinetic model. Different isotherm models were applied to experimental data, while the Sips isotherm model best describes the equilibrium of the adsorption process on the tested modified material. According to this isotherm model, the maximum achieved adsorption capacities of Cu(II), Zn(II), and Se(IV) were 48.21, 55.06, and 87.85 mg/g, respectively. The summarized experimental results revealed that the adsorption process of selected cations on modified OS was predominantly caused by chemisorption, while, in addition to chemisorption, electrostatic forces were also responsible for Se(IV) removal. Desorption test showed that the prepared material could be reused for at least 3 cycles, with minimal efficiency loss. Briefly, this study reinforces that DES-modified agro-waste biomass could be used as a promising adsorbent for cations and oxyanions from wastewater.

Keywords: waste biomass; metals and metalloids removal; DES modification; adsorption mechanism

1. Introduction

Water pollution caused by industrial effluent discharge into natural watercourses becomes a significant global problem. Various physical, chemical, or biological pollutants pose a serious risk to human health, animals, and the environment. Due to their persistency, non-degradability, high toxicity even at low concentrations, and bioaccumulation, heavy metals in industrial effluents pose a potential threat to the environment and living organisms [1–3]. For these reasons, there is an urgent global demand to find an appropriate method for purifying industrial wastewater containing heavy metals before its discharge. So far, numerous different purification methods, such as coagulation, flocculation, membrane filtration, and chemical precipitation, have been utilized [2]. However, these traditional methods exhibit certain operational drawbacks that hinder the motivation for their application.

For this reason, novel, environmentally acceptable techniques for wastewater treatment are considered. Among all the techniques, adsorption has been recognized as a highly selective, efficient, and cost-effective technology for pollutant removal from aqueous effluents. In recent decades, the application of natural materials as adsorbents has attracted increasing scientific attention.

Recently, the exploitation of waste biomass as an adsorbent has become particularly attractive due to the valorization of low-cost, easily available, renewable, and sustainable materials [1]. Numerous different waste materials were investigated as potential biosorbents. Thus, Fan et al. used weed as an efficient adsorbent for Cu ion removal [4], while Aguilar et al. utilized waste coffee pulp, banana pseudo-stem, and corn cob as potential Zn adsorbents [5]. Previous research revealed that waste biomass as an adsorbent material displays high efficiency due to its large surface area, porosity, low mass, and unique properties. The surface of such adsorbents is abundant with functional groups, such as carboxyl, phenolic, and amine, which represent suitable sites for pollutants binding through hydrogen bonds, electrostatic interactions, and coordinated bond formation [6]. One of the advantages of waste biomass utilization is the ability to combust used material before its disposal, and thus reduce the amount of waste that needs to be managed. Besides, waste biomass after the regeneration of metals from its surface can be further converted to value-added carbon-rich materials.

Concerning additional enhancement of sorption ability, previous studies recommended different methods of tailoring the biomass's structure in order to increase surface area and provide more binding sites. In order to achieve improvement, biomass is often modified with alkaline solutions. Consequently, Simić et al. [1] achieved a 2.23-times higher capacity of corn silk for Cd(II) ion removal after modification with KOH. Neem biomass chemically pretreated with NaOH and citric acid was confirmed as an efficient biosorbent to remove Pb(II) ions from aqueous solutions [7]. However, recently attention has been devoted to deep eutectic solvents (DES) as innovative green solvents for lignocellulose biomass treatment to procure the desired characteristics for potential further application. The adoption of DES for these purposes has numerous advantages, among which are high chemical and thermal stability, high purity, nontoxicity, high ionic strength, low volatility, recyclability, and high biodegradability [8,9]. DES is composed of hydrogen bond donors and acceptors, which provide the ability to fractionate biomass, especially due to its high solubility of lignin. After DES treatment, a more porous and accessible cellulose structure remains in comparison to raw biomass and is therefore a more suitable material for further applications [10].

Oat straw is a low-cost, widely available waste co-product that is left behind after the harvesting of oat (*Avena sativa*) [11]. Since waste straw is produced in large quantities during agri-food processing to reduce environmental impact and create economic value, its appropriate utilization is of great importance. For this reason, numerous studies have investigated its potential applications. Consequently, Borrega et al. [11] investigated the potential valorization of oat straw as an alternative source of lignocellulosic fibers. On the other hand, Szufa et al. [12] have considered oat straw after torrefaction treatment as a potential energy source and additive to organic fertilizers, while Onyenwoke et al. [13] applied steam explosion pretreatment to oat straw to improve the quality of biofuel pellets generated from these feedstocks. In addition to the mentioned applications, it should consider the potential utilization of waste oat straw as an adsorbent of various pollutants, primarily heavy metals. Although oat husks have been investigated as potential biosorbents of heavy metals from aqueous solutions, there is a lack of data on the valorization of oat straw as a sorbent in the literature. As for other lignocellulosic biomaterials, the main constituents of straw are macromolecules such as lignin, cellulose, and hemicellulose. These constituents are available for interaction with different pollutants and thus provide potential and promising adsorption materials. In addition to lignocellulose, this material also contains minerals such as magnesium, calcium, and sodium, which contribute to ion exchange with selected pollutants [14].

The main ambition of this study is the valorization of waste oat straw as a novel bio-based sorbent for highly toxic pollutants (Cu(II), Zn(II), and Se(IV)). In order to improve its adsorption properties and applicability, for the first time in the literature, DES (L-arginine + choline chloride/urea) modification of oat straw was applied. Two particular objectives were achieved by DES treatment: (i) degradation of the rigid and complex

lignocellulosic structure of biomass and/or (ii) functionalization of the oat surface with new functional groups. In order to investigate the influence of the treatment on the morphological properties of the resulting bio-based sorbent, detailed pHpzc, SEM, FTIR, and DSC/TG characterizations were performed. According to the results of adsorption studies, the maximum adsorption capacities were determined, as were the mechanisms responsible for the binding of selected pollutants onto the modified oat straw surface. Furthermore, comprehensive conclusions about interactions and differences between the binding of cations and oxyanion at DES-modified biomass are drawn. A summarized result from this work provides a reference for the preparation of a novel, efficient bio-based adsorbent from waste lignocellulosic biomass.

2. Materials and Methods

2.1. Chemicals

All chemicals and reagents used in this study were of analytical grade. Primary stock solutions (1000 mg/L) of Cu(II), Zn(II), and Se(IV) were prepared by dissolving appropriate amounts of selected salts ($Cu(NO_3)_2 \times 3H_2O$, $ZnSO_4 \times 7H_2O$, and Na_2O_3Se, respectively) in ultra-distilled water. Desired concentrations of working solutions were obtained by dilutions of the primary stock solutions. Additional chemicals supplied by Sigma-Aldrich included absolute ethanol, choline chloride, and amino acid arginine, which were used for DES preparation.

2.2. Biomass Preparation

The initial biomass exploited in this study was oat straw waste. The sample was obtained from the local field in Banat (a region in Serbia) after harvesting in 2021. The biomass was collected, washed in order to remove traces of soil and other impurities from the surface, and air-dried at room temperature. Thereafter, the biomass was ground, sieved, and oven-dried at 105 °C until it reached a constant weight. In all experiments, a sieved fraction of 63–125 μm was used. The prepared biomass sample (OS) was placed in a sealed container and used in further experiments.

2.3. Biomass Modification

In order to partially degrade lignocellulosic constituents, the OS was modified using DES prepared by cholinium arginate ionic liquid (IL) and urea. The synthesis of selected DES followed the combined procedures previously reported by Liu et al. (2012) and Wang et al. [15,16]. Briefly, an ethanol mixture that contains potassium hydroxide and choline chloride (1:1 molar ratio) was heated at 60 °C, agitated for 4 h, and vacuum filtrated. Upon vacuum filtration, a selected amino acid (arginine) was added to a liquid phase and stirred at room temperature. Thereafter, the thus prepared ionic liquid was combined with urea (2:1 molar ratio), stirred at 60 °C for 2 h, and dried to produce DES. In order to prepare the desired concentration of aqueous DES solution, the crude DES was dissolved in a water/ethanol mixture.

During the next step, 1 g of the OS was modified using 10 mL of prepared DES solution. The contact was achieved by stirring for 4 h at 40 °C. After the reaction period, the mixture was filtered, and the produced modified biomass (IOS) was washed several times with a mixture of water and ethanol, dried, and used in subsequent adsorption experiments.

2.4. Material Characterization

The point of zero charge (pHpzc) of materials before and after DES modification was determined according to a method previously proposed by Milonjic et al. [17]. Based on this method, pHpzc values of selected OS and IOS (0.01 g) were determined in 0.001 M and 0.01 M KNO_3 solutions at selected ranges (2.0 to 12.0 (pH_i)). The pHi values were adjusted using 0.01 M HNO_3 and/or 0.01 M KOH solutions. After a reaction period of 24 h, the final pH (pH_f) was measured, and the diagram (pH_f vs pH_i) was created to determine the pHpzc.

In order to determine the structural differences caused by modification, detailed characterizations of OS and IOS were performed. Surface characterization was performed by FTIR analysis using the Thermo Scientific Nicolet iS50 FTIR spectrometer. Analyzed samples were prepared by mixing 0.8 mg of the OS or IOS with 80 mg of KBr and recording in the 4000 to 400 cm^{-1} spectral range.

Additionally, the morphological characteristics of the samples were examined by scanning electron microscopy (SEM) using Jeol JSM-6610 LV at 20 keV. Prior to recording, all samples were dried at 105 °C overnight, coated with gold, and placed on an adhesive carbon disc.

The thermal stability of OS and IOS was predicted by differential scanning calorimetry coupled with thermogravimetric analysis (DSC/TG) using a Netzsch STA 449 F5 Jupiter. Approximately 5 mg of each tested sample was heated in alumina cups up to 900 °C at a heating rate of 10 °C/min under an inert atmosphere.

2.5. Ultrasound and Water Stability Test of IOS

The stability of the IOS materials was determined by an ultrasonic bath at different time periods. The influence of ultrasound was tested on the investigated adsorbent material to investigate its stability under vibrations that can penetrate the deepest pores of the material and cause partial or complete erosion [18]. The influence of ultrasound was tested using Bandelin Sonorex (Bandelin, Typ: RK 102 H, Berlin, Germany). Briefly, 0.1 g of each sample was displayed at a frequency of 35 kHz for 0.5 and 1 h. Besides, to reveal the water stability of IOS, 0.1 g of material was dispersed in 100 mL of ultrapure water during 24, 48, 72, and 96 h of exposure [19]. The mass of dry samples before and after stability tests was measured and compared.

2.6. Adsorption Study

To gain insight into the influence of modification processes on adsorbent efficiency, a preliminary adsorption test using OS and IOS was performed. For this purpose, a dose of 0.1 g/L of each sorbent was added to 1 mM solutions of Cu, Zn, and Se, respectively. The contact was established for 24 h, and after the reaction period, the amounts of the remaining metal ions and oxyanions in the filtrates were monitored. In order to further optimize the adsorption conditions and examine the removal mechanism, various adsorption tests were performed in anionic and cationic solutions using IOS. For this purpose, different operational parameters, which include the pH value of the initial solution, contact time, and initial pollutant concentration, were varied. During Cu(II) and Zn(II) adsorption tests, an adsorbent dose of 1 g/L was used, while Se(IV) removal was tested with a sorbent dose of 0.5 g/L. The influence of pH was measured at different pH values of initial pollutants solutions (1 mM Cu(II), Zn(II), and Se(IV) solutions were used), which ranged from 2 to 6 for Cu(II) and Zn(II), and from 2 to 9 for Se(IV), for 24 h. In addition, for batch kinetic experiments, a selected dose of adsorbent was stirred with a 1 mM pollutant solution at pH 5 for Cu(II) and Se(IV) and pH 4 for Zn(II) at various time intervals (from 15 to 1440 min), while the concentration ranges of 0.2 to 2 mM (Cu(II), Zn(II), and Se(IV)) at pH 4 (Zn(II)) and pH 5(Cu(II) and Se(IV)) were used to explore the influence of initial concentrations. Batch adsorption experiments were performed in 100 mL Erlenmeyer flasks placed on top of a Heidolph Unimak1010 orbital shaker and agitated (220 rpm) at room temperature. At the end of the experiments, the metal concentration in the filtered aliquots was measured by AAS (Perkin Elmer 900T, Waltham, MA, USA). Besides, all adsorption tests were carried out in triplicate, and the average values of the obtained results are shown.

The amounts of adsorbed contaminants were estimated using the following equation:

$$q_e = (C_i - C_e) \times V/m \tag{1}$$

where q_e represents the amount of adsorbed metal on the IOS (mg/g), C_i and C_e are initial and equilibrium metal concentrations (mg/L), respectively, V is the volume of the metal solution (L), and m is the mass of the IOS (g).

The desorption performance of the IOS was revealed through cyclic adsorption experiments. Briefly, 0.1 M HNO3 and 0.1 M EDTA solutions were used as desorption agents. After the adsorption cycle, 0.05 g of IOS was stirred for 180 min with 50 mL of each desorption solution, filtered, rinsed with ultrapure water, dried, and applied in the following sorption/desorption cycle [4,6]. All testes desorption agents were performed during three cycles. The qeq values were monitored after each cycle.

To investigate adsorption kinetics and isotherm models, linear and non-linear fitting methods were employed using Origin 9.0 software.

To examine the possible ion-exchange mechanism during the adsorption of Cu(II), Zn(II), and Se(IV) ions, filtrates upon adsorption are subjected to determination of the released cations (Ca^{2+}, Mg^{2+}, K^+, Na^+, and H^+). The influence of van der Waals forces was eliminated by using a control sample (filtrate) obtained by mixing IOS in ultrapure water at pH 5.0. The materials were shaken for 24 h at 220 rpm at room temperature. The content of Ca^{2+}, Mg^{2+}, K^+, and Na^+ in the resulting filtrates was monitored using an atomic absorption spectrophotometer (AAS) (Analytic Jena Spekol 900T, Jena, Germany), while the content of H^+ ions was determined from the difference in pH values between the control and filtrate after adsorption.

A real-sample analysis was conducted on industrial process water rich in copper. During the adsorption test, 20 mL of the real sample and 0.02 g of IOS were stirred for 24 h at 220 rpm at room temperature. The pH value of the real sample was not adjusted; it was just monitored.

3. Results

3.1. Material Characterization

Scanning electron microscopy analysis was utilized to examine the morphology of the tested OS and IOS. The results displayed in Figure 1 reveal that the pristine OS had a continuous and flat structure with notable channels and cracks through the whole surface, characteristic of lignocellulosic biomass [1]. On the other hand, Figure 1b implies that increased surface area was achieved upon DES modification treatment. As is already known, the DES treatment leads to the degradation of the structural constituents of lignocellulosic biomass, and thus new materials with improved adsorption performances are obtained [20]. Accordingly, the relatively smooth surface of the OS becomes significantly disorganized after modification. Numerous channels and irregularities, as well as a much rougher heterogeneous structure compared to the native material, are noticeable (Figure 1b). The formation of porous structures after the modification of hazel with an ionic liquid was observed by Gollakota et al. [3]. In addition, the appearance of new cracks ensures a better diffusion of ions during the contact of metal solutions with the material surface. The obtained results are in accordance with previous studies, which confirmed that biomass modification caused similar surface disarrangement and improved adsorption performances for metal ion removal [1,20].

In order to examine the changes in the chemical structure of native OS caused by DES modification, FTIR analysis was performed. The FTIR spectra before and after modification are presented in Figure 2a. As can be seen, the spectrum of OS contains peaks characteristic of lignocellulosic biomass. The wide peak at 3355 cm^{-1} originated from stretching and flexural vibrations of hydrogen bonds from the O–H group, while the peak that appears at 2918 cm^{-1} can be ascribed to symmetric C–H valence vibrations from cellulose, hemicellulose, and lignin [21,22]. Furthermore, the peaks at 1600, 1258, 1162, 1110, 1054, and 1035 cm^{-1} indicate the presence of hydrogen-containing functional groups, such as COO-, C–O, and/or C–O–C, while the peaks at 1458 and 1375 cm^{-1} implied the presence of C–H bends from lignin, cellulose, and hemicellulose [21,23–25]. The FTIR spectra of the OS also exhibit peaks at 1647 and 1507 cm^{-1}, which originated from aromatic rings and the C=C bonds. Moreover, the C–H deformation from aromatic skeletal vibrations from lignocellulosic structures was confirmed by bands that appear at 1425, 1321, and 898 cm^{-1} [21,23–25].
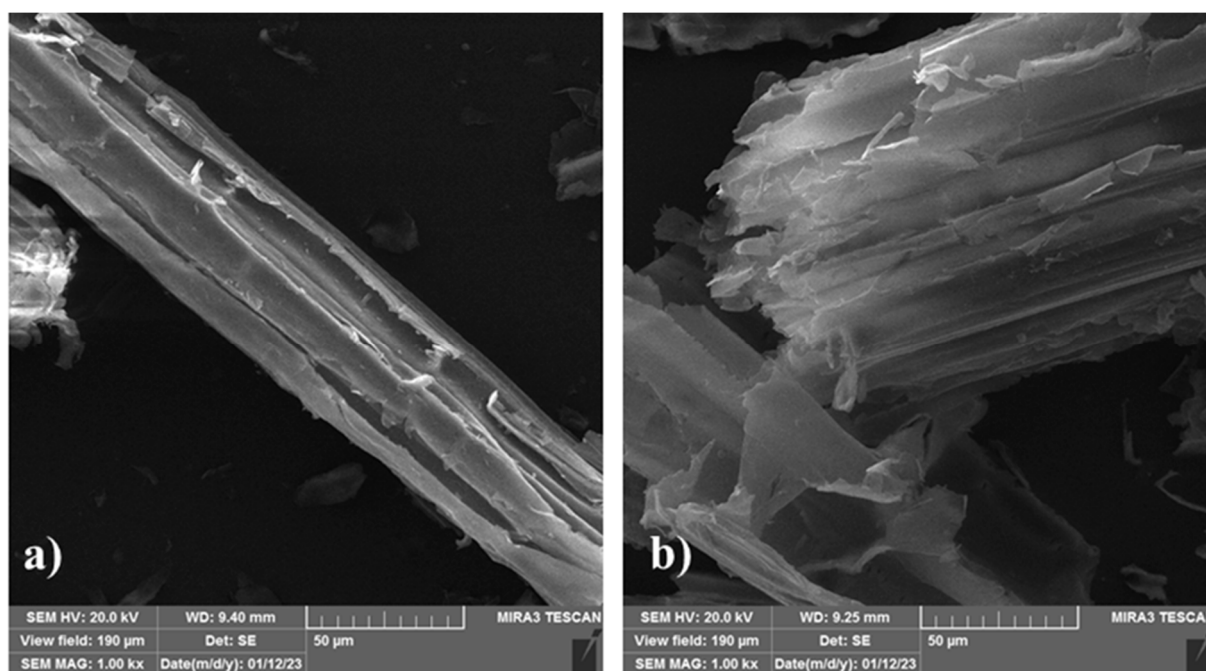
Figure 1. SEM images of the OS (**a**) before and (**b**) after DES modification.
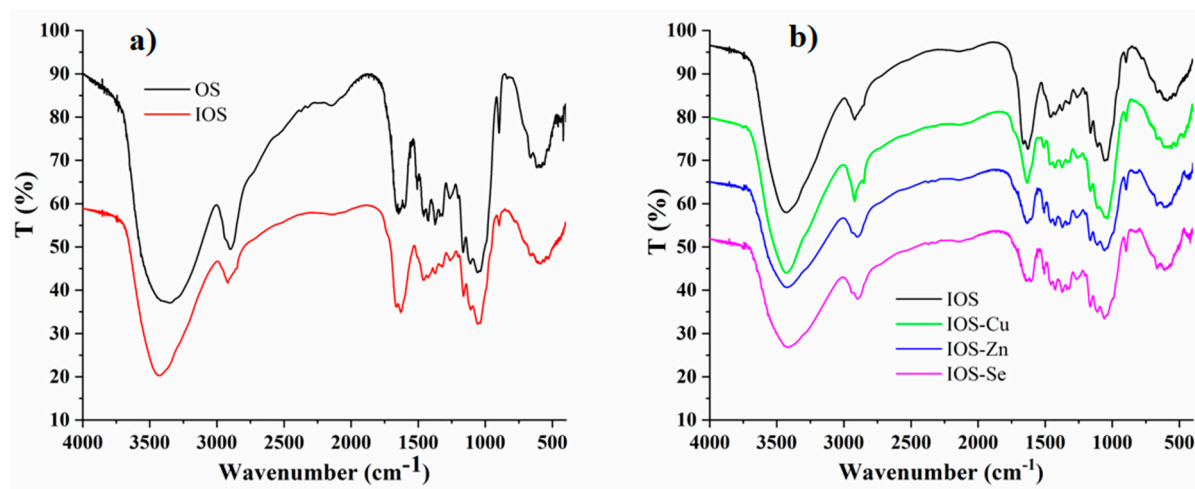
Figure 2. FTIR spectra of (**a**) OS and IOS and (**b**) IOS after adsorption.

Due to its remarkable performances, DES was able to significantly change the structure of lignocellulosic biomass through the degradation of structural constituents of biomass [8,9]. These allegations were confirmed in this study. As can be seen from Figure 2a, notable changes in the FTIR spectrum have been observed after DES modification. Decreased peak intensity or complete disappearance indicates degradation or removal of lignocellulose structures from the OS sample [22]. Similar findings were reported previously during the treatment of peanut shell and miscanthus, respectively, with ionic liquids [21,22]. Besides the important peaks that confirm the successful incorporation of DES onto the IOS surface, they are noticed at around 1600 cm^{-1} (skeletal stretching vibrations of C=N bonds) [26].

Differences caused by metal binding on the IOS surface are presented in Figure 2b. The changes in certain peaks in FTIR spectra involved in pollutant bindings were displayed. It was observed that the wide peak from the O–H, visible at 3355 cm^{-1} was reduced. This reduction is most pronounced after the sorption of Se(IV) ions. Peaks at 1400–1000 cm^{-1}, attributed to COO-, C–O, C–O–C, aliphatic and aromatic C-H bonds, as well as N-containing

functional groups (1600 cm^{-1}), also exhibited reduced intensity. Their reduction and shift towards lower wavenumbers indicate the involvement of oxygen, nitrogen, and aromatic functional groups in chemical interactions with tested pollutants [1,24]. This observation is particularly noticeable during Se(IV) removal. This is a sign of one of the proposed binding mechanisms: complexation with oxygen and nitrogen functional groups followed by H$^+$ release. According to these observations, a proposed mechanism may include the π–π interaction between aromatic groups of IOS (C=C and –CH) and ions, electrostatic interaction between surface functional groups of IOS, and surface complexation between oxygen and nitrogen-containing functional groups on the IOS surface and selected pollutants.

Additionally, the OS and IOS samples were analyzed by DSC/TG. Based on the results presented in the diagrams (Figure 3), it is possible to compare and draw conclusions about the difference in mass change in TG and thermal change in DSC analysis for OS and IOS.
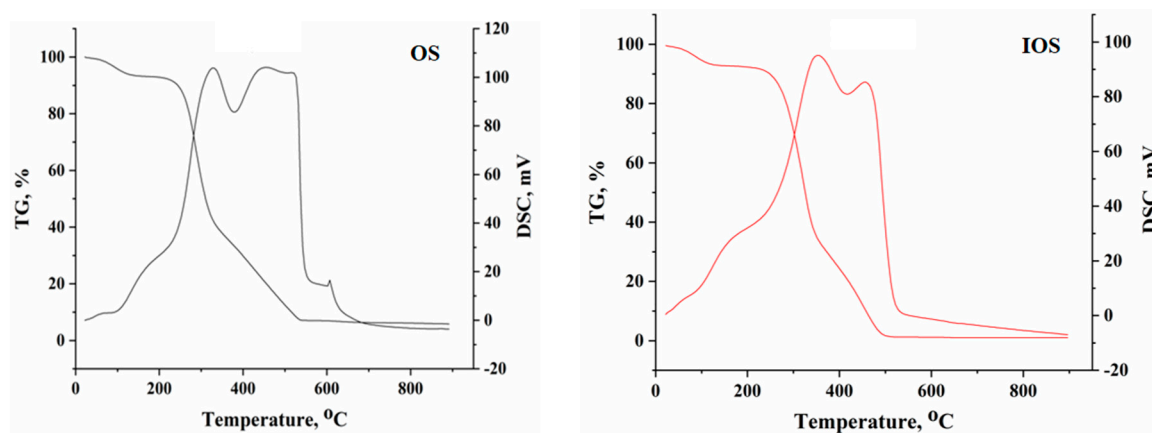
Figure 3. The DSC/TG diagrams of OS and IOS.

The DSC/TG diagrams implied that the OS and IOS have three distinct reaction zones. The first zone on the TG diagram originated from the weight losses (6.70 and 6.83% for OS and IOS, respectively) caused by water evaporation [12,27]. The second weight loss that starts at 200 °C indicates that degradation of the biomass structural constituents (lignin, cellulose, and hemicellulose) has begun [27,28]. Firstly, the decomposition of OS and IOS starts slowly, while intensive mass losses caused by volatilization of structural components become more pronounced at 260 °C (55.43 and 57.53%, for OS and IOS, respectively). The third phase covers the range from 360 to 530 °C for the OS sample. In the case of the IOS sample, this phase ends before 530 °C, which indicates a lower lignin content compared to the OS sample [28]. In addition, the weight loss of both samples reaches more than 90% at 600 °C, and this is in agreement with previous literature data [29]. The residual weight loss for the OS and IOS samples was 5.79% and 1.02%, respectively. According to the obtained results, it can be concluded that partial lignin degradation has occurred as a result of DES modification.

In addition, the first stage in the DSC diagrams (up to 150 °C) represents water evaporation and small organic molecules volatilization [12,27]. The peaks at the diagram interval from 300 to 550 °C originated from the degradation of lignocellulosic constituents of biomass [28,30]. It is known that thermal treatment causes degradation of the lignocellulosic materials, firstly volatilized hemicellulose, followed by cellulose, while lignin is the most thermally stable [31]. Thus, for the OS sample, the exothermic peak with a maximum peak at 323 °C may be attributed to the degradation of hemicellulose, while the broad, overlapped peak at 454 °C indicates oxidation of cellulose and lignin [28]. A final sharp peak observed at 608 °C originated from inorganics incorporated in the biomass structure [32].

As a result of the modification process, a clear peak separation on the IOS DSC diagram is observed. In addition, the maximum of the first peak is shifted from 329 °C towards 353 °C, suggesting the degradation of hemicellulose. Besides, the second broad peak

became sharper and exhibited reduced intensity. These phenomena indicate that during the modification, partial degradation of lignin occurred. The absence of a small, sharp peak at 608 °C in the IOS sample might be associated with the leaching of inorganic components due to DES treatment. Biomass dissolution, i.e., activation, during ionic liquid treatment was also confirmed by Labbé et al. [30].

3.2. Ultrasound and Water Stability of IOS

The influence of water exposure time on the stability of IOS materials is shown through the percentage of mass loss. The obtained results showed that there was no significant weight loss of the IOS sample and that after 96 h of exposure to water, a weight reduction of only 1.07% was observed. In addition, ultrasonic stability showed similar results. After 0.5 h of exposure of IOS material to a frequency of 35 kHz, there was a negligible loss of mass (0.20%), and after 1 h, the mass loss was 0.96%. Based on the obtained results, we can conclude that there is no significant material degradation, and therefore IOS exhibits stability in water and during exposure to ultrasonic waves.

3.3. Batch Adsorption Tests

3.3.1. Preliminary Adsorption Test

The preliminary adsorption test (Figure 4) revealed a significant improvement in the adsorption capacity after modification, so further adsorption tests considered the ability of the material as an adsorbent for selected metals and metalloids (Cu(II), Zn(II), and Se(IV)) were performed only using IOS.
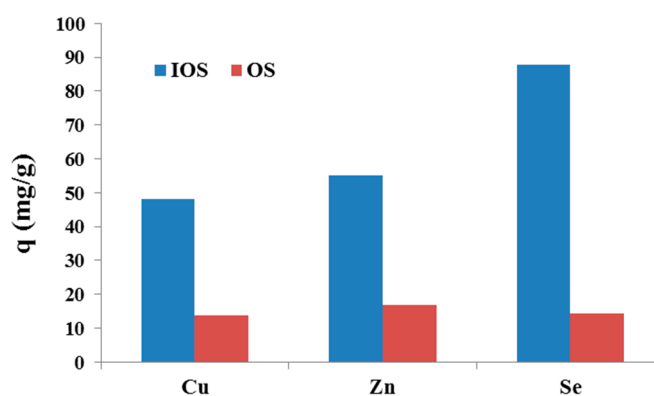
Figure 4. Preliminary adsorption test using OS and IOS.

3.3.2. The Effect of Initial pH

The initial pH value of the solution governs the adsorbent surface charge as well as the ionization degree of the tested pollutant, so it represents one of the important factors that influence adsorption efficiency. Thus, the effect of the solution pH value during the removal of Cu(II) and Zn(II) using IOS was tested in a range of 2 to 6, while a pH range of 2 to 9 was adopted for Se(IV) removal (Figure 5). The obtained results show that the increase in pH value led to a consequent increase in adsorption capacity. The reason for the hindered removal at lower pH is competition between H^+ ions and metal ions for active sites on the surface of the IOS. However, an increase in pH led to the reduction of H^+ ions in the solution, while the functional groups on the IOS surface became deprotonated and accessible for the binding of positively charged ions. Accordingly, the maximum adsorption capacities (40.5 mg/g for Cu(II) and 47.5 mg/g for Zn(II)) were achieved between pH 4 and 5 for divalent metal ions (Figure 5). The observed adsorption trend is consistent with previous studies that examined the removal of heavy metals from aqueous solutions using modified biomass [1]. On the other hand, the removal of Se(IV) as an oxyanion shows a slightly different trend. As Figure 5 reveals, better removal is achieved at lower pH values, while the highest adsorption capacity is achieved at pH 5. A further pH value increase causes a rapid decrease in capacity, probably due to a competition of OH^- ions with

Se(IV) oxyanions for the available binding sites on the IOS surface. Similar observations were previously reported by Jevtić et al. during the removal of Se(IV) using Fe-modified zeolites [33]. Subsequent adsorption experiments were performed at pH values at which the maximum capacities for the tested ions were obtained.
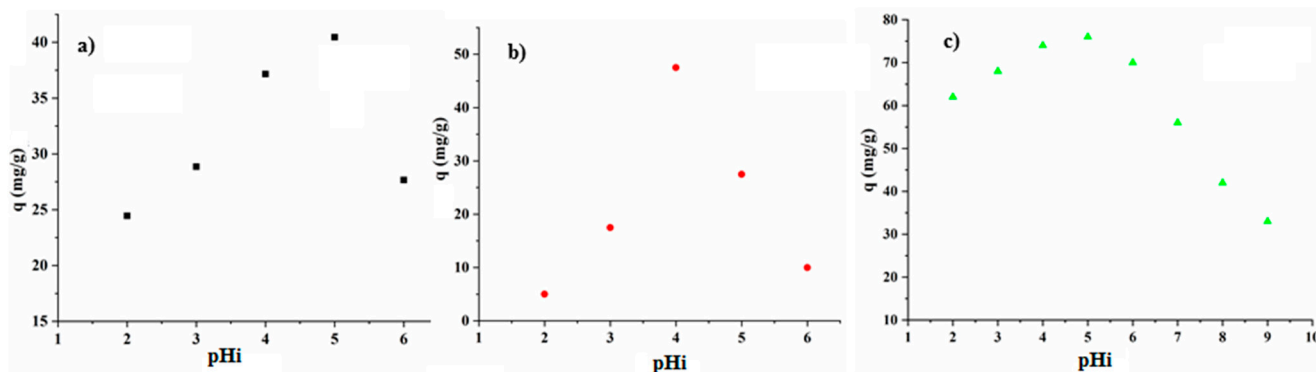
Figure 5. Influence of pH on (**a**) Cu(II), (**b**) Zn(II), and (**c**) Se(IV) ion removal using IOS. (T = 25 °C, C_0 = 1 mM, t = 1440 min, adsorbent dosage = 1 g/L for Cu(II), Zn(II), and 0.5 g/L for Se(IV)).

The neutral value of the surface charge is determined by the point of zero charge (pHpzc). According to pHpzc, the adsorbent surface charge is positive and could interact with negatively charged ions at a pH lower than pHpzc; on the contrary, a negative surface charge is achieved at a pH higher than pHpzc. The knowledge gained from the pHpzc may indicate the involvement of possible electrostatic interactions between the adsorbent surface and ions in solution [1,26].

The OS and IOS values of pHpzc were found to be 7.0 and 9.48, respectively. Besides, the value of pHpzc is almost the same for both tested KNO_3 concentrations, indicating the independence of pHpzc in relation to the ionic strength of the background electrolyte. A higher value of pHpzc suggests a more alkaline surface of IOS upon DES treatment.

The adsorption of Cu(II), Zn(II), and Se(IV) on the IOS reaches its maximum at pH < pHpzc (Figure S1). At this pH value, the surface of the modified material is positively charged, indicating that during the removal of positively charged cations (Cu(II) and Zn(II)), electrostatic forces do not play a significant role, but they are involved in the interaction of the IOS surface with negatively charged oxyanions (Se(IV)) [1,26]. This could be an additional explanation for why the adsorption capacity for Se(IV) removal is higher in comparison to Cu(II) and Zn(II).

3.3.3. Effect of Contact Time and Kinetics Studies

The effect of contact time was examined in order to define the equilibrium time of metal ion sorption at the IOS surface. The reduced concentration trends of the investigated ions were monitored during a period of time from 15 to 1440 min. The results are shown in Figure 5. During the initial time interval, fast sorption was observed for all tested ions; thus, almost 50% of Cu(II), Zn(II), and Se(IV) ions were removed in the first 15 min. This occurrence is most likely the result of the interface of ions with the available active sites on the adsorbent surface [34]. After this period, adsorption capacity gently grows until the equilibrium of the system is reached. The equilibrium capacities of Cu(II), Zn(II), and Se(IV) ions were 42.16, 34.5, and 81 mg/g, respectively. Their equilibriums were reached for 360 min (Figure 6).
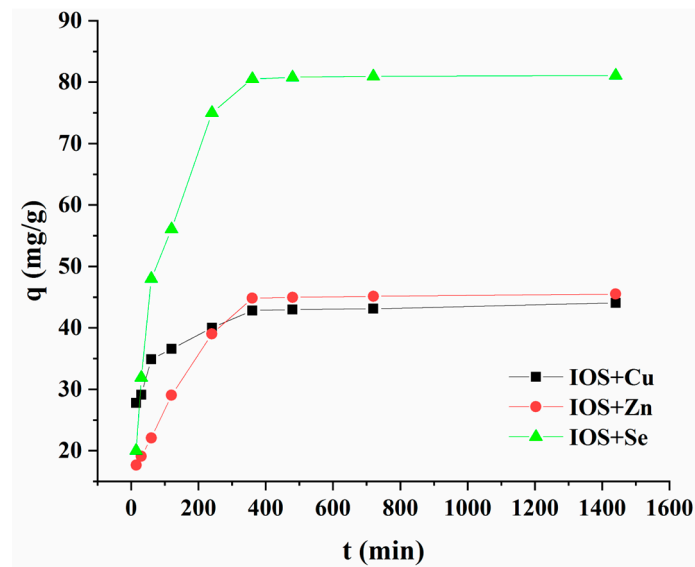
Figure 6. The effect of contact time during Cu(II), Zn(II), and Se(IV) ions removal using IOS (pH 5. for Cu(II) and Se(IV), pH 4 for Zn(II), T = 25 °C, C_0 = 1 mM adsorbent dosage = 1 g/L for Cu(II), Zn(II), and 0.5 g/L for Se(IV)).

Adsorption kinetic studies provide further information about metal ion binding mechanisms, sorption rates, and potential rate-limiting steps. For that purpose, kinetic models that include the pseudo-first-order [35], pseudo-second-order [36], and Weber–Morris intraparticle diffusion [37] models were applied to the obtained experimental data. The linear model equations are listed below:

The pseudo-first-order rate equation:

$$\frac{1}{q_t} = \left(\frac{k_1}{q_{eq}}\right)\left(\frac{1}{t}\right) + \left(\frac{1}{q_{eq}}\right) \tag{2}$$

The pseudo-second-order rate equation:

$$\frac{t}{q_t} = \left(\frac{1}{k_2 q_{eq}^2}\right) + \left(\frac{1}{q_{eq}}\right)t \tag{3}$$

The intra-particle diffusion model equation:

$$q_t = K_{id}t^{0.5} + C \tag{4}$$

where q_{eq} and q_t are the amount of pollutant adsorbed at equilibrium and time t using IOS (mg/g) at equilibrium and time t. The k_1 (1/min), k_2 (g/mg min^{-1}), and K_{id} (mg/g min$^{-1/2}$) represent the pseudo-first-order, pseudo-second-order, and intra-particle diffusion rate constants, respectively, while C is the intercept.

The adsorption plots of pseudo-second-order and intra-particle diffusion kinetic models are shown in Figure 7, while calculated parameters are summarized and displayed in Table 1. According to the results shown in Table 1, it can be concluded that the values of the correlation coefficient (R^2) for Cu(II), Zn(II), and Se(IV) ions were higher and closer to 1 for the pseudo-second-order kinetic model. These observations indicate that the removal kinetics of all selected pollutants onto the IOS surface follow the proposed model. This conclusion is supported by the fact that the calculated equilibrium adsorption capacities obtained from the pseudo-second model were in agreement with experimentally achieved values ($q_{eq,exp}$) (Table 1). The pseudo-second-order model implies that chemical interactions between pollutant ions and the IOS surface are crucial for metal ion binding. These conclusions are in accordance with the results obtained by FTIR analysis in this study. Simi-

larly, Zhang et al. [2] also concluded that chemisorption is the rate-controlling step during the adsorption of Cu(II) and Pb(II) ions using ionic liquid@porous organic frameworks. Besides, Jevtić et al. and Marjanović et al. have shown that the removal of Se(IV) ions from aqueous solutions also follows a pseudo-second-order kinetic model [33,38].
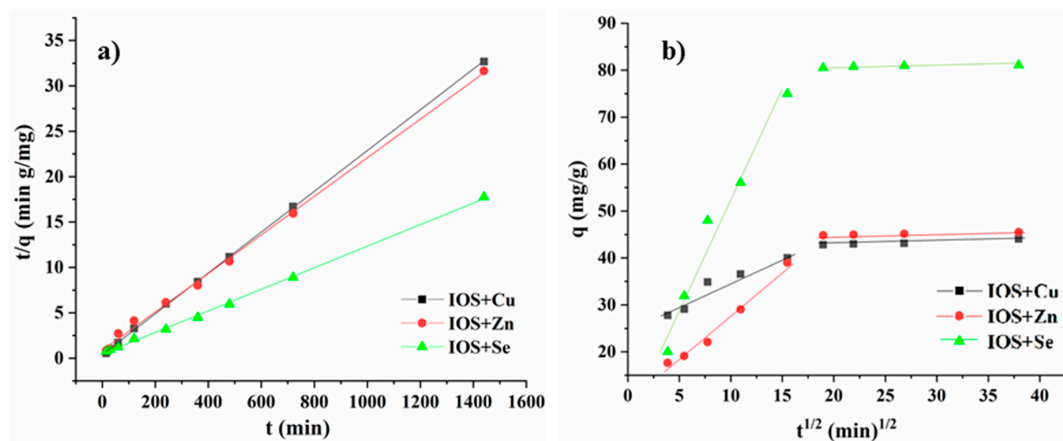
Figure 7. Kinetic adsorption curves for pollutants adsorption onto IOS: (**a**) pseudo-second-order; (**b**) Weber–Morris intra-particle diffusion. (pH 5 for Cu(II) and Se(IV), pH 4 for Zn(II), T = 25 °C, C_0 = 1 mM adsorbent dosage = 1 g/L for Cu(II), Zn(II), and 0.5 g/L for Se(IV)).

Table 1. Kinetic parameters for Cu(II), Zn(II), and Se(IV) removal on IOS.

Adsorbent IOS	Cu	Zn	Se
$q_{eq, exp}$ [mg/g]	42.16 ± 0.51	34.5 ± 1.25	79.90 ± 2.10
Pseudo-First-Order Model			
q_{eq} [mg/g]	41.49 ± 0.84	40.13 ± 0.99	86.73 ± 1.85
k_1 [1/min]	8.95 ± 0.25	23.20 ± 0.36	50.35 ± 0.69
R^2	0.8757 ± 0.08	0.8073 ± 0.05	0.9974 ± 0.008
Pseudo-Second-Order Model			
q_{eq} [mg/g]	44.52 ± 0.52	47.07 ± 1.02	83.47 ± 0.99
k_2 [g/mg min^{-1}]	0.0545 ± 0.004	0.0251 ± 0.001	0.0254 ± 0.0015
R^2	0.9998 ± 0.0001	0.9978 ± 0.002	0.9988 ± 0.0001
Weber–Morris diffusion Model			
K_{id1} [mg/g min$^{-1/2}$]	1.0662 ± 0.032	1.8833 ± 0.22	4.5293 ± 0.85
C_1 [mg/g]	24.3892 ± 0.014	8.9812 ± 0.84	6.7541 ± 1.23
R^2	0.9255 ± 0.022	0.9830 ± 0.023	0.9669 ± 0.036
K_{id2} [mg/g min$^{-1/2}$]	0.0658 ± 0.001	0.0355 ± 0.001	0.0253 ± 0.008
C_2 [mg/g]	41.5664 ± 1.25	44.1516 ± 0.98	80.1554 ± 0.97
R^2	0.9619 ± 0.015	0.9995 ± 0.00	0.8798 ± 0.053

In addition, the Weber–Morris intra-particle diffusion model was included to examine the impact of intra-particle diffusion on removal processes (Figure 7b). Figure 7b reveals that split linear zones are attended to for all ion removal processes. According to these findings, it can be concluded that intra-particle diffusion is not the only rate-determining step, but several mechanisms interfere with the adsorption of the tested ions. Similar perceptions were previously described by Simić et al. [1] and Zhang et al. [2].

3.3.4. Isotherm Study

In order to define the equilibrium of Cu(II), Zn(II), and Se(IV) adsorption on IOS, the obtained experimental data were fitted by Langmuir, Freundlich, Sips, and Redlich–Peterson isotherm models. Generally, isotherms can provide insight into the nature of interaction between the pollutant and adsorbent materials surfaces, and thus allow the assumption of a possible binding mechanism [26].

The Langmuir model explains monolayer adsorption at a fixed number of active sites and follows Equation (5) [39]:

$$q_e = q_{max}K_LC_e/(1 + K_LC_e) \tag{5}$$

where q_{max} is the maximal amount of pollutant adsorbed using IOS (mg/g), and K_L is the Langmuir constant (L/mg).

The feasibility and favorability of pollutant adsorption can be described by the dimensionless constant (R_L) [40]:

$$R_L = 1/(1 + K_LC_0) \tag{6}$$

where R_L is the separation factor. The biosorption process on the IOS is: unfavorable if the $R_L > 1$; linear if the $R_L = 1$; favorable if the $0 < R_L < 1$; or irreversible if the $R_L = 0$ [41].

The Freundlich isotherm explains multilayer adsorption at the heterogeneous surface. The following equation expresses this model [42]:

$$Qe = K_FCe^{1/n} \tag{7}$$

where K_F (mg/g (mg/L)$^{-1/n}$) and $1/n$ are the Freundlich constants. If the n_F value is between 1 and 10, it can be concluded that the adsorption of Cu(II), Zn(II), and Se(IV) on IOS is favorable.

The Sips isotherm model predicts the Freundlich isotherm at low pollutant concentrations, while at high pollutant concentrations, it predicts the Langmuir isotherm model. It can be expressed by Equation (8) [43]:

$$q_e = q_{max}(K_SC_e)^{1/ns}/(1 + (K_SC_e)^{1/nS}) \tag{8}$$

where K_S (mg/L)$^{-1/n}$ and $1/n_S$ are the Sips constants. A higher value of the n_S parameter predicts adsorption onto a more heterogeneous system.

The Redlich–Peterson isotherm model implies homogeneous monolayer adsorption with constant enthalpies and adsorption energies [26]. The Redlich–Peterson isotherm model is usually expressed by the following equation [44]:

$$q_e = K_{RP}C_e/(1 + a_{RP}C^g_e) \tag{9}$$

where K_{RD} and a_{RP} represent Redlich–Peterson constants (L/g) and ((mg/L)$^{-g}$), respectively, and g is an empirical Redlich–Peterson parameter ($g \leq 1$).

Equilibrium data were fitted to the abovementioned isotherm models, and the coefficient of determination (R^2) values were the criteria used for model selection. The fitted isotherm models of Cu(II), Zn(II), and Se(IV) adsorption on the IOS are presented in Figure 8, while Table 2 contains the calculated parameters.
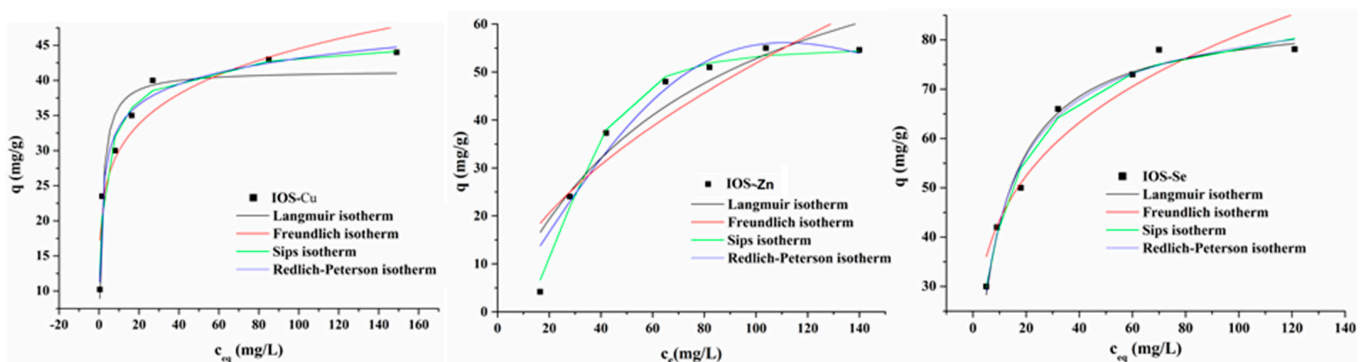
Figure 8. Non-linear fits of different isotherm models to the Cu(II), Zn(II), and Se(IV) adsorption by IOS (pH 5 for Cu(II) and Se(IV), pH 4 for Zn(II), T = 25 °C, t = 1440 min, adsorbent dosage = 1 g/L for Cu(II), Zn(II), and 0.5 g/L for Se(IV)).

Table 2. Parameters and determination coefficients of the isotherm models.

Models	Parameters	Cu	Zn	Se
Langmuir	q_m (mg/g)	41.41 ± 2.15	99.12 ± 5.28	85.89 ± 1.98
	K_L (L/mg)	0.70 ± 0.02	0.01 ± 0.001	0.09 ± 0.01
	R^2	0.9347 ± 0.0021	0.8890 ± 0.0013	0.9813 ± 0.0028
	R_L	0.010 ± 0.001	0.42 ± 0.02	0.066 ± 0.001
	χ^2	8.27 ± 0.08	4.79 ± 0.04	8.13 ± 0.02
Freundlich	K_F (mg/g)(L/mg)$^{1/n}$	20.21 ± 1.18	3.68 ± 0.45	23.33 ± 1.26
	$1/n$	5.83 ± 1.02	1.74 ± 0.15	3.71 ± 0.78
	R^2	0.8959 ± 0.0127	0.8203 ± 0.0098	0.9281 ± 0.0104
	χ^2	18.48 ± 1.89	7.77 ± 0.98	31.33 ± 2.45
Sips	q_m (mg/g)	48.21 ± 1.98	55.06 ± 2.18	87.85 ± 4.24
	K_S (L/mg)	0.58 ± 0.09	0.00003 ± 0.00001	0.12 ± 0.01
	n_s	0.58 ± 0.08	0.98 ± 0.11	0.86 ± 0.09
	R^2	0.9818 ± 0.14	0.9931 ± 0.11	0.9838 ± 0.12
	χ^2	1.20 ± 0.23	3.73 ± 0.89	8.81 ± 1.12
Redlich–Peterson	K_{RP} (L/g)	49.67 ± 1.78	0.83 ± 0.05	9.30 ± 0.78
	a_{RP} (L/mg)	1.68 ± 0.21	0.0005 ± 0.00001	0.12 ± 0.01
	β	0.91 ± 0.11	0.51 ± 0.08	0.96 ± 0.15
	R^2	0.9771 ± 0.0213	0.9471 ± 0.0199	0.9821 ± 0.0214
	χ^2	5.82 ± 0.45	28.60 ± 1.15	9.70 ± 0.98

According to the data from Table 2, it can be concluded that the Langmuir equation provides a practical description of the experimental data and suggests monolayer adsorption onto the IOS. In addition, values of R_L and $1/n$ are between 0–1 and 0–10, respectively, indicating favorable adsorption of Cu(II), Zn(II), and Se(IV) removal utilizing the IOS. Moreover, the favorability of the adsorption of Cu(II), Zn(II), and Se(IV) onto the investigated IOS is also confirmed by other calculated parameters summarized in Table 2 that imply this statement: the $K_L < 1$, $K_F > 1$, $\beta < 1$, and n_s values are in the range from 0 to 1 [1,26].

Moreover, from the values of the R^2 and nonlinear chi-square (χ^2) values obtained from the isothermal study, it can be suggested that the Sips isotherm model best describes the adsorption of selected pollutants on the IOS surface. This isotherm model proposes that the maximum adsorption capacities achieved for Cu(II), Zn(II), and Se(IV) removal using IOS are 48.21, 55.06, and 87.85 mg/g, respectively. In addition, the removal efficiency achieved in this study for IOS was better than or comparable with other materials previously investigated for Cu(II), Zn(II), and/or Se(IV) adsorption (Table 3). Besides, the heterogeneity of the IOS surfaces is confirmed by the value of the $1/n_S$ parameter that is bigger than 1. As can be seen, the best adsorption capacity was achieved during Se(IV) removal. During the DES modification, the amino groups were attached to the OS surface (FTIR analysis confirms this assumption), and their presence can be a reason for the highest Se(IV) adsorption in comparison to Cu(II) and Zn(II). Moreover, the efficiency of the IOS as a bio-based adsorbent towards Se(IV) ions tested in this study was better than that of Fe-modified zeolites (21.6 mg/g) [33].

Table 3. Adsorption capacity of different sorbents towards Cu(II), Zn(II), and/or Se(IV) ions.

Adsorbent	q_m (mg/g)			Reference
	Cu(II)	Zn(II)	Se(IV)	
Plant-crofton weed	33.87			[4]
Eggshell	34.48	35.71		[45]
Sugarcane bagasse	3.65	40.00		[45]
Corn silk (*Zea mays L.*)	15.35	13.98		[46]
Coffee pulp		13.53		[5]
NaOH modified Agave bagasse		20.24		[47]

Table 3. *Cont.*

Adsorbent	q_m (mg/g)			Reference
	Cu(II)	**Zn(II)**	**Se(IV)**	
S. cerevisiae biomass			39.00	[48]
Green algae			74.90	[49]
Iron(III)-modified zeolitic Fe-CLI			21.60	[33]
Modified lignin microspheres			69.90	[38]
IOS	48.21	55.06	87.85	This study
OS	13.76	16.85	14.25	This study

3.3.5. Desorption Study

The adsorption/desorption ability was tested and calculated for each of the three cycles and displayed in Figure 9. As Figure 9 shows, tested desorption agents maintain high ion removal efficiency. The adsorption capacity for Cu(II), Zn(II), and Se(IV) slightly decreases with cycles, but capacity did not drop more than 10%. Besides, HNO_3 proved to be a slightly better desorption agent than the EDTA solution. Since desorption efficiency after tree cycles was more than 90%, it can be concluded that IOS can be effectively regenerated.
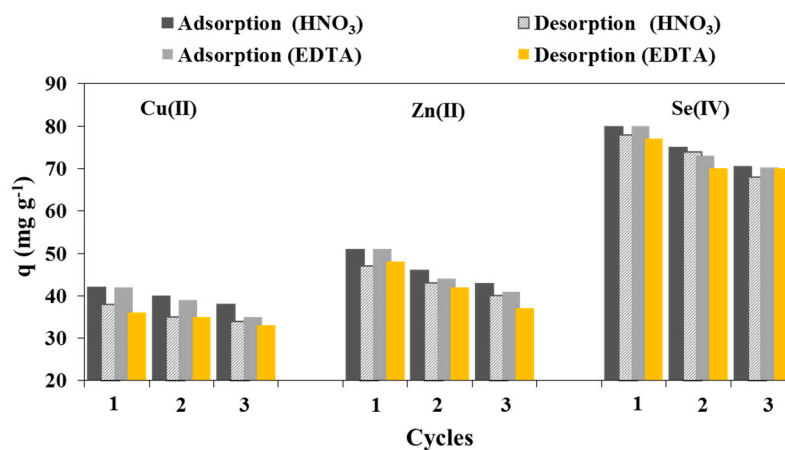
Figure 9. Adsorption/desorption cycles using HNO_3 and EDTA as desorption agents.

3.3.6. Ion-Exchange Mechanism

The ion exchange mechanism represents the exchange of ions between the solid material surfaces and ions from the liquid phase. It is one of the main mechanisms responsible for the adsorption of metal ions from solution [1,26]. In this research, the mechanism of ion exchange on the adsorption of Cu(II), Zn(II), and Se(IV) ions was examined according to the ratio of adsorbed metal ions and the released cations from the tested adsorbent surface [26,46]. The amounts of adsorbed pollutants and released Ca(II), Mg(II), Na(I), K(I), and H(I) at different solution concentrations are given in Figure 10. From the obtained results, it can be seen that the amount of bonded Cu(II), Zn(II) and Se(IV) ions increases with increasing concentration of the solution up to 1 mM, after which there are no significant changes. The release of Ca(II), Mg(II), Na(I), and K(I) ions indicates the formation of an ionic bond, while the exchange of H(I) ions favors covalent bonding. During the removal of Cu(II) and Zn(II) ions, Ca(II), and K(I) ions were the most significantly involved in ion exchange, followed by Mg(II), while the involvement of Na(I) and H(I) ions was negligible. Besides, the amount of cations released from the IOS adsorbent is less than the amount of adsorbed ions, which indicates that other mechanisms besides ion exchange are involved in the removal of selected metals. The summarized findings from this paper confirm this allegation. This is especially noticeable during the Se(IV) ion removal because it binds in the form of an oxyanion and creates complexes. The most exchangeable ion during Se(IV)

removal is Na(I), while the participation of other ions is much smaller. The obtained results revealed that the ion-exchange mechanism is definitely involved in the binding of selected cations and oxyanion to the IOS surface.
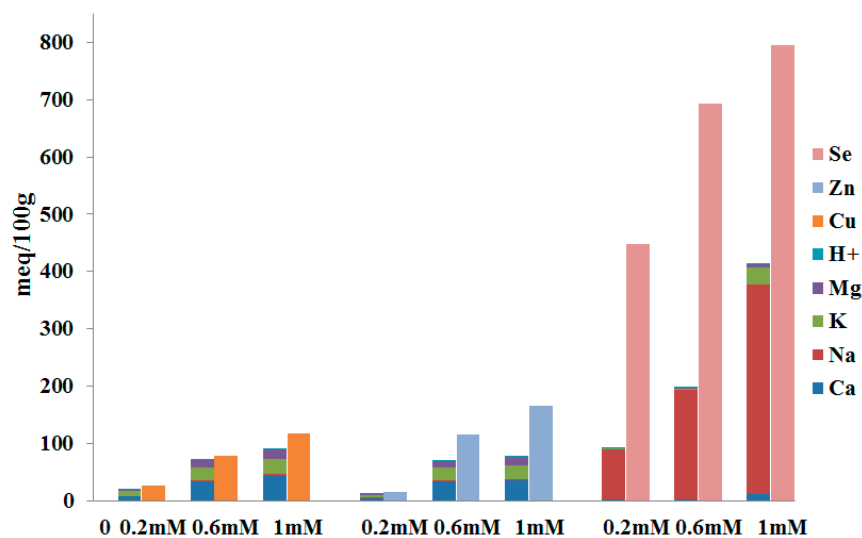
Figure 10. The amounts of adsorbed Cu(II), Zn(II), and Se(IV) and amounts of released Ca(II), Mg(II), Na(I), K(I), and H(I) at different initial metal concentrations.

3.3.7. Real Effluent Analysis

The application of the IOS sample as an adsorbent for the removal of Cu(II), Zn(II), and/or Se(IV) metals from industrial wastewater was tested. For the purpose of printing, tap water was taken from the pre-processing metal industry in Serbia. Metal concentrations in wastewater before (IWW) and after adsorption (IWW-IOS) were measured using an AAS method. The obtained experimental results are shown in Table 4. There were no Se(IV) ions in the tested wastewater. The pH value of industrial wastewater was 3. The IOS adsorbent reduces the concentration of Cu(II) and Zn(II) ions as well as other present ions in the solution. The lower adsorption of ions compared to the data obtained from single metal experiments is probably due to the competition of ions in a solution with a low pH. This is in agreement with our previously obtained results from testing the influence of the solution's pH value on the sorption capacity. In this multimetallic solution, the highest removal was achieved for Zn(II) ions. Based on the obtained data, we can conclude that IOS can be used as a potential adsorbent for the removal of Cu(II) and Zn(II) ions from industrial wastewater.

Table 4. Real effluent before and after removal of metals by IOS.

	Cu(mg/L)	Zn(mg/L)	Pb(mg/L)	Cd(mg/L)	Ni(mg/L)	Fe(mg/L)
IWW	6.62	6.05	4.7	0.16	0.4	0.94
IWW-IOS	3.54	2.12	3.3	0.06	0.1	0.45

4. Conclusions

In this study, OS modified with DES was utilized for potential Cu(II), Zn(II), and Se(IV) remediation. Results of structural characteristics (SEM, FTIR, and DSC/TG) reveal that selected biomass treatments caused partial degradation of lignocellulosic constituents and incorporated novel functional groups onto the OS surface. FTIR analysis confirmed the involvement of oxygen and nitrogen functional groups, as well as aromatic C=C, in the binding of selected pollutants. Besides, pHpzc indicates the involvement of electrostatic interactions in the case of Se(IV) removal. The modification process increases adsorption capacities by more than four times. Adsorption of Cu(II), Zn(II), and Se(IV) using IOS was

achieved through two simultaneous stages, while chemisorption was the rate-controlling step. The isotherm study reveals that favorable adsorption originated on the monolayer heterogeneous surface of the IOS. The maximum adsorption capacities from the Sips isotherm model were 48.21, 55.06, and 87.85 mg/g for Cu(II), Zn(II), and Se(IV), respectively. Moreover, the adsorption mechanism reveals that π–π interaction, electrostatic interaction, ion exchange, and surface complexation are involved in the binding of selected pollutants during their contact with the IOS surface.

In general, this study reinforces that the investigated synthesized materials could be used as promising adsorbents for heavy metals and oxyanions in wastewater treatment. Moreover, utilization of the DES modification process provides facile, green, and economical methods for improving agro-waste into high-value bio-based adsorbents.

Supplementary Materials: The following supporting information can be downloaded at: https://www.mdpi.com/article/10.3390/pr11051308/s1, Figure S1: pHpzc for OS and IOS.

Author Contributions: Conceptualization, J.D., M.S. and J.P.; methodology, S.J.; software, M.K.; validation, M.K.; formal analysis, J.D.; investigation, J.D., S.J. and J.P.; resources, A.M. and S.J.; data curation, M.S.; writing—original draft preparation, J.D. and S.J.; writing—review and editing, M.S., J.P. and A.M.; visualization, M.S; supervision, S.J. and A.M. All authors have read and agreed to the published version of the manuscript.

Data Availability Statement: Not applicable.

Conflicts of Interest: The authors declare no conflict of interest.

References

1. Simić, M.; Petrović, J.; Šoštarić, T.; Ercegović, M.; Milojković, J.; Lopičić, Z.; Kojić, M. A Mechanism Assessment and Differences of Cadmium Adsorption on Raw and Alkali-Modified Agricultural Waste. *Processes* **2022**, *10*, 1957. [CrossRef]
2. Zhang, T.; Jiang, W.; Cao, Y.; Zhu, C.; Toukouki, S.; Yao, S. A facile one-pot synthesis of ionic liquid@porous organic frameworks for rapid high-capacity removal of heavy metal ions, pesticides and aflatoxin from two non-food bioactive products. *Ind. Crop. Prod.* **2022**, *181*, 114859. [CrossRef]
3. Gollakota, R.K.A.; Munagapati, S.V.; Shu, M.C.; Wen, C.J. Adsorption of Cr (VI), and Pb (II) from aqueous solution by 1-Butyl-3-methylimidazolium bis(trifluoromethylsulfonyl)imide functionalized biomass Hazel Sterculia (*Sterculia foetida* L.). *J. Mol. Liq.* **2022**, *350*, 118534. [CrossRef]
4. Fan, L.; Miao, J.; Yang, J.; Zhao, X.; Shi, W.; Xie, M.; Wang, X.; Chen, W.; An, X.; Luo, H.; et al. Invasive plant-crofton weed as adsorbent for effective removal of copper from aqueous solution. *Environ. Technol. Innov.* **2022**, *26*, 102280. [CrossRef]
5. Aguilar, G.L.D.; Rodríguez Miranda, P.J.; Miller, A.X.M.; Astudillo, M.I.R.; Muñoz, E.A.J. Removal of Zn(II) in Synthetic Wastewater Using Agricultural Wastes. *Metals* **2020**, *10*, 1465. [CrossRef]
6. Chen, Y.; Chen, Q.; Zhao, H.; Dang, J.; Jin, R.; Zhao, W.; Li, Y. Wheat Straws and Corn Straws as Adsorbents for the Removal of Cr(VI) and Cr(III) from Aqueous Solution: Kinetics, Isotherm, and Mechanism. *ACS Omega* **2020**, *5*, 6003–6009. [CrossRef] [PubMed]
7. Hatiya, A.N.; Reshad, S.A.; Negie, W.Z. Chemical Modification of Neem (*Azadirachta indica*) Biomass as Bioadsorbent for Removal of Pb^{2+} Ion from Aqueous Waste Water. *Adsorpt. Sci. Technol.* **2022**, *2022*, 7813513. [CrossRef]
8. Zhang, Y.; Meng, Y.; Ma, L.; Ji, H.; Lu, X.; Pang, Z.; Dong, C. Production of biochar from lignocellulosic biomass with acidic deep eutectic solvent and its application as efficient adsorbent for Cr (VI). *J. Clean. Prod.* **2021**, *324*, 129270. [CrossRef]
9. Xu, H.; Dong, C.; Wang, W.; Liu, Y.; Li, B.; Liu, F. Machine learning prediction of deep eutectic solvents pretreatment of lignocellulosic biomass. *Ind. Crop. Prod.* **2023**, *196*, 116431. [CrossRef]
10. Jose, D.; Tawai, A.; Divakaran, D.; Bhattacharyya, D.; Venkatachalam, P.; Tantayotai, P.; Sriariyanun, M. Integration of deep eutectic solvent in biorefining process of lignocellulosic biomass valorization. *Bioresour. Technol. Rep.* **2023**, *21*, 101365. [CrossRef]
11. Borrega, M.; Hinkka, V.; Hörhammer, H.; Kataja, K.; Kenttä, K.; Ketoja, A.J.; Palmgren, R.; Salo, M.; Sundqvist-Andberg, H.; Tanaka, A. Utilizing and Valorizing Oat and Barley Straw as an Alternative Source of Lignocellulosic Fibers. *Materials* **2022**, *15*, 7826. [CrossRef]

12. Szufa, S.; Wielgosiński, G.; Piersa, P.; Czerwińska, J.; Dzikuć, M.; Adrian, L.; Lewandowska, W.; Marczak, M. Torrefaction of Straw from Oats and Maize for Use as a Fuel and Additive to Organic Fertilizers—TGA Analysis, Kinetics as Products for Agricultural Purposes. *Energies* **2020**, *13*, 2064. [CrossRef]

13. Onyenwoke, C.; Tabil, G.L.; Dumonceaux, T.; Cree, D.; Mupondwa, E.; Adapa, P.; Karunakaran, C. Investigation of Steam Explosion Pretreatment of Sawdust and Oat Straw to Improve Their Quality as Biofuel Pellets. *Energies* **2022**, *15*, 7168. [CrossRef]

14. Kosiorek, M.; Wyszkowski, M. Content of macronutrients in oat (*Avena sativa* L.) after remediation of soil polluted with cobalt. *Environ. Monit. Assess.* **2019**, *191*, 389. [CrossRef] [PubMed]

15. Liu, P.Q.; Hou, D.X.; Li, N.; Zong, H.M. Ionic liquids from renewable biomaterials: Synthesis, characterization and application in the pretreatment of biomass. *Green Chem.* **2012**, *14*, 304–307. [CrossRef]

16. Wang, Y.; Zhang, J.W.; Yang, J.Y.; Li, M.L.; Peng, F.; Bian, J. Efficient fractionation of woody biomass hemicelluloses using cholinium amino acids-based deep eutectic solvents and their aqueous mixtures. *Bioresour. Technol.* **2022**, *354*, 127139. [CrossRef] [PubMed]

17. Milonjić, S.K.; Ruvarac, A.L.; Šušić, M.V. The heat of immersion of natural magnetite in aqueous solutions. *Thermochim. Acta* **1975**, *11*, 261–266. [CrossRef]

18. Breitbach, M.; Bathen, D. Influence of ultrasound on adsorption processes. *Ultrason. Sonochemistry* **2001**, *8*, 277–283. [CrossRef]

19. Li, Q.; Li, R.; Ma, Z.; Zhang, W.; Sarkar, B.; Sun, X.; Bolan, N. Efficient removal of antimonate from water by yttrium-based metal-organic framework: Adsorbent stability and adsorption mechanism investigation. *Colloids Surf. A Physicochem. Eng. Asp.* **2022**, *633*, 127877. [CrossRef]

20. Lai, P.; Zhou, H.; Niu, Z.; Li, L.; Zhu, W.; Dai, L. Deep eutectic solvent-mediated preparation of solvothermal carbon with rich carboxyl and phenol groups from crop straw for high-efficient uranium adsorption. *Chem. Eng. J.* **2023**, *457*, 141255. [CrossRef]

21. Babicka, M.; Woźniak, M.; Bartkowiak, M.; Peplińska, B.; Waliszewska, H.; Zborowska, M.; Borysiak, S.; Ratajczak, I. Miscanthus and Sorghum as sustainable biomass sources for nanocellulose production. *Ind. Crop. Prod.* **2022**, *186*, 115177. [CrossRef]

22. Lawal, I.A.; Chetty, D.; Akpotu, S.O. Moodley, Sorption of Congo red and reactive blue on biomass and activated carbon derived from biomass modified by ionic liquid. *Environ. Nanotechnol. Monit. Manag.* **2017**, *8*, 83–91. [CrossRef]

23. Dehkhoda, S.; Bagher, M.; Heydari, M. Extraction of carboxylated nanocellulose from oat husk: Characterization, surface modification and in vitro evaluation of indomethacin drug release. *Int. J. Biol. Macromol.* **2022**, *212*, 165–171. [CrossRef] [PubMed]

24. Ying, D.; Hlaing, M.M.; Lerisson, J.; Pitts, K.; Cheng, L.; Sanguansri, L.; Augustin, M.A. Physical properties and FTIR analysis of rice-oat flour and maize-oat flour based extruded food products containing olive pomace. *Int. Food Res. J.* **2017**, *100*, 665–673. [CrossRef]

25. Kubovský, I.; Kačíková, D.; Kačík, F. Structural Changes of Oak Wood Main Components Caused by Thermal Modification. *Polymers* **2020**, *12*, 485. [CrossRef]

26. Petrović, J.; Ercegović, M.; Simić, M.; Kalderis, D.; Koprivica, M.; Milojović, J.; Radulović, D. Novel Mg-doped pyro-hydrochars as methylene blue adsorbents: Adsorption behavior and mechanism. *J. Mol. Liq.* **2023**, *376*, 121424. [CrossRef]

27. Ghaly, A.E.; Ergüdenler, A.; Al Taweel, A.M. Determination of the kinetic parameters of oat straw using thermogravimetric analysis. *Biomass Bioenergy* **1993**, *5*, 457–465. [CrossRef]

28. Mlonka-Mędrala, A.; Evangelopoulos, P.; Sieradzka, M.; Zajemska, M.; Magdziarz, A. Pyrolysis of agricultural waste biomass towards production of gas fuel and high-quality char: Experimental and numerical investigations. *Fuel* **2021**, *296*, 120611. [CrossRef]

29. Mukhambet, Y.; Shah, D.; Tatkeyeva, G.; Sarbassov, Y. Slow pyrolysis of flax straw biomass produced in Kazakhstan: Characterization of enhanced tar and high-quality biochar. *Fuel* **2022**, *324*, 124676. [CrossRef]

30. Nicole Labbé, N.; Kline, M.L.; Moens, L.; Kim, K.; Kim, C.P.; Hayes, G.D. Activation of lignocellulosic biomass by ionic liquid for biorefinery fractionation. *Bioresour. Technol.* **2012**, *104*, 701–707. [CrossRef] [PubMed]

31. Garcia-Maraver, A.; Salvachúa, D.D.; Martínez, M.J.; Diaz, F.L.; Zamorano, M. Analysis of the relation between the cellulose, hemicellulose and lignin content and the thermal behavior of residual biomass from olive trees. *Waste Manag.* **2013**, *33*, 2245–2249. [CrossRef] [PubMed]

32. Bi, H.; Ni, Z.; Tian, J.; Wang, C.; Jiang, C.; Zhou, W.; Bao, L.; Sun, H.; Lin, Q. The effect of biomass addition on pyrolysis characteristics and gas emission of coal gangue by multi-component reaction model and TG-FTIR-MS. *Sci. Total Environ.* **2021**, *798*, 149290. [CrossRef]

33. Jevtić, S.; Arčon, I.; Rečnik, A.; Babić, B.; Mazaj, M.; Pavlović, J.; Matijašević, D.; Nikšić, M.; Rajić, N. The iron(III)-modified natural zeolitic tuff as an adsorbent and carrier for selenium oxyanions. *Microporous Mesoporous Mater.* **2014**, *197*, 92–100. [CrossRef]

34. Petrović, J.; Stojanović, M.; Milojković, J.; Petrović, M.; Šoštarić, T.; Laušević, M.; Mihajlović, L.M. Alkali modified hydrochar of grape pomace as a perspective adsorbent of Pb^{2+} from aqueous solution. *J. Environ. Manag.* **2016**, *182*, 292–300. [CrossRef]

35. Lagergren, S. Zur theorie der sogenannten adsorption gelöster stoffe. *K. Sven. Vetenskapsakad. Handl.* **1898**, *24*, 1–39. [CrossRef]

36. Ho, Y.S.; McKay, G. Pseudo-second order model for sorption processes. *Process. Biochem.* **1999**, *34*, 451–465. [CrossRef]

37. Weber, W.; Morris, J. Kinetics of adsorption on carbon from solution. *J. Sanit. Eng. Div.* **1963**, *89*, 31–60. [CrossRef]

38. Marjanović, V.; Radmila Marković, R.; Steharnik, M.; Dimitrijević, S.; Marinković, D.A.; Perić-Grujić, A.; Đolic, M. Lignin Microspheres Modified with Magnetite Nanoparticles as a Selenate Highly Porous Adsorbent. *Int. J. Mol. Sci.* **2022**, *23*, 13872. [CrossRef] [PubMed]

39. Langmuir, I. The adsorption of gases on plane surfaces of glass, mica and platinum. *J. Am. Chem. Soc.* **1918**, *40*, 1361–1403. [CrossRef]
40. Webber, T.W.; Chakkravorti, R.K. Pore and solid diffusion models for fixed-bed adsorbers. *AlChE J.* **1974**, *20*, 228–238. [CrossRef]
41. Foo, K.Y.; Hameed, B.H. Insights into the modeling of adsorption isotherm systems. *Chem. Eng. J.* **2010**, *156*, 2–10. [CrossRef]
42. Freundlich, H.M.F. Über die adsorption in lösungen. *Z. Phys. Chem.* **1906**, *57A*, 385–470. [CrossRef]
43. Sips, R. On the structure of a catalyst surface. *J. Chem. Phys.* **1948**, *16*, 490–495. [CrossRef]
44. Redlich, O.; Peterson, D. A useful adsorption isotherm. *J. Phys. Chem.* **1959**, *63*, 1024–1027. [CrossRef]
45. Putra, P.W.; Kamari, A.; Yusoff, S.N.M.; Ishak, C.F.; Mohamed, A.; Hashim, N.; Isa, I.M. Biosorption of Cu(II), Pb(II) and Zn(II) Ions from Aqueous Solutions Using Selected Waste Materials: Adsorption and Characterisation Studies. *J. Encapsulation Adsorpt. Sci.* **2014**, *4*, 25–35. [CrossRef]
46. Petrović, M.; Šoštarić, T.; Stojanović, M.; Petrović, J.; Mihajlović, M.; Ćosović, A.; Stanković, S. Mechanism of adsorption of Cu^{2+} and Zn^{2+} on the corn silk (*Zea mays* L.). *Ecol. Eng.* **2017**, *99*, 83–90. [CrossRef]
47. Velazquez-Jimenez, H.L.; Pavlick, A.; Rangel-Mendez, J.R. Chemical characterization of raw and treated agave bagasse and its potential as adsorbent of metal cations from water. *Ind. Crop. Prod.* **2013**, *43*, 200–206. [CrossRef]
48. Khakpour, H.; Younesi, H.; Mohammadhosseini, M. Two-stage biosorption of selenium from aqueous solution using dried biomass of the baker's yeast Saccharomyces cerevisiae. *J. Environ. Chem. Eng.* **2014**, *2*, 532–542. [CrossRef]
49. Tuzen, M.; Sarı, A. Biosorption of selenium from aqueous solution by green algae (*Cladophora hutchinsiae*) biomass: Equilibrium, thermodynamic and kinetic studies. *Chem. Eng. J.* **2010**, *158*, 200–206. [CrossRef]